AI-based Technique to Enhance Transient Response and Resiliency of Power Electronic Dominated Grids via Grid-Following Inverters

Mohsen Hosseinzadehtaher, *Student Member, IEEE*, Alireza Zare, *Student Member, IEEE*, Ahmad Khan, *Student Member, IEEE*, Muhammad F. Umar, *Student Member, IEEE*, Silvanus D'silva, *Student Member, IEEE*, and Mohammad B. Shadmand, *Senior Member, IEEE*

Abstract—This paper presents a frequency restoration method to enhance power electronic dominated grid (PEDG) resiliency and transient response via re-defining grid following inverters (GFLIs) role at the grid-edge. An artificial intelligence-based power reference correction (AI-PRC) module is developed for GFLIs to autonomously adjust their power setpoints during transient disturbances. A detailed analytical validation is provided that shows control rules in PEDG intrinsically follow the underlying dynamic of the swing-based machines to extend its stability boundary. Considering this fact, comprehensive transient and steady state-based mathematical models are used for constructing the learning database of the proposed AI-PRC. The proposed training approach can deal with grid's characteristics alterations and uncertainties. Thus, this approach incorporates PEDG's effective variables that shapes its dynamic response during transient disturbances. Subsequently, a neural network is trained by Bayesian regularization algorithm (BRA) to realize the proposed AI-PRC scheme for frequency support via GFLIs. Several simulation and experimental case studies results validate the functionality of the proposed AI-PRC towards enhancing the PEDG's transient response and resiliency via GFLIs. The provided case studies demonstrate significant improvement in frequency restoration in response to transient disturbances.

Keywords– power electronic dominated grid, resiliency, Bayesian regularization algorithm, artificial neural network, transient stability.

I. INTRODUCTION

The increased contribution of renewable-based energy resources for maintaining sustainable and clean energy utilization in the modernized power system is affecting the grid conventional operation methodologies. Power electronic dominated grids (PEDGs) suffer from the lack of minimum mandatory inertia requirements for maintaining the grid stability [1, 2]. Specifically, frequency and voltage stability are vulnerable in low inertia networks [3]. Equivalent system inertia and short circuit ratio (SCR) are the parameters that have more influence on the resiliency and stability boundary of the PEDG [4]. Thus, system frequency, rate of change of frequency (ROCOF) and voltage stability may get jeopardized due to potential transient disturbances. Likewise, due to the intermittent nature of renewable energy-based sources, restoring the frequency excursion to the nominal is a major challenge to ensure stable operation of the PEDG in real-time.

Typically, grid forming inverters (GFMIs) have the mainstream contributions for sustaining transient stability when a disturbance takes place in the system, and this is due to their characteristic obligations [5]. Moreover, in the steady state condition, GFMIs are responsible for sharing the total system load among each other [6]. However, these GFMIs have restrictions in terms of loading capacities especially when large disturbances occurs either on demand side or supply side. Thus, if they are coerced to contribute to a specific loading condition more than their nominal rating, the inverter cannot provide a proper dynamic response which could results in significant stability issues in PEDG. Also, having numerous GFMIs operating in parallel can be problematic due to the possibility of power circulating amongst them and synchronization challenges [7, 8]. However, by implementing a sort of synthetic droop control which is predominantly adopted from the primary frequency control loop of a synchronous generator (SG), the total load can be shared among the inverters while the grid's voltage and frequency are regulated autonomously.

On the other hand, grid following inverters (GFLIs) can be employed to strengthen the upstream grid voltage and frequency by equipping their control loops with droop fundamentals [8, 9] or a supervisory control system [10] instead of maximum power point operation [11, 12]. To benefit from the GFLIs to enhance system resiliency during disturbances, it is vital to add up another outer loop of voltage and frequency control. The active power is adjusted based on a thorough *P-f* control gain and the reactive power is regulated by using another gain that relates the voltage magnitude to the required reactive power. It is essential to realize accurate gains which are contingent on quite a few other parameters such as the grid's physical features and the intensity of disturbances. Irrespective of grid forming or grid following inverters, if the *P-f* droop coefficient is slightly decreased, the ROCOF can be intensified while faster frequency regulation can be achieved. Therefore, a challenging tradeoff is needed in selection process of these parameters. Moreover, the cut-off frequency of the employed low-pass filter in control loop of GFLIs plays a significant role in its stability. Considering the same constraint for droop coefficient in GFMI and GFLI, varying the cut-off frequency has an explicit influence on the ROCOF and frequency as well. Thus, frequency and voltage restoration can be a challenging task in a PEDG.

A variety of basic to advanced frequency restoration control approaches are developed in the literature. The notion of virtual synchronous generator (VSG) can be implemented in GFMI and GFLI to relatively damp system oscillatory transients due to the external disturbances with lower uncertainty regarding the stability violation [13]. In [14], a nonlinear control technique is introduced to expand the transient stability boundary which is extremely influenced by the frequency dynamics of the system. The authors proposed that in VSG-based control schemes, the

inertial value cannot be assumed as a constant and a correlation should be established between the frequency excursion and inertia constant. In fact, the performance of the proposed approach in [14] doesn't properly meet the IEEE 1547 standard regarding the ROCOF constraints. Consequently, it is crucial to have a faster frequency detection scheme. A droop-based approach in combination with ROCOF control for providing the active power set point in the event of frequency excursion is presented in [15] with the goal of adopting SG-based frequency control with extensive mechanical and electrical models. It is worthy to mention that the conventional droop and VSG based controls are not able to pick up the load for distinct dynamic characteristics either in grid-tied or standalone mode of operation at the same time.

A comparison has been conducted on the dynamic response of VSG and droop-based control schemes in [16, 17]. Both control approaches are based on the droop fundamentals. It should be noticed that a droop-based control characteristically does not emulate system inertia. Nevertheless, by employing delay in their control loops, the system can emulate the virtual inertia. As mentioned in [18], VSG and inertia droop-based controls can take the advantage of the droop features and simultaneously add virtual inertia to the operating grid. However, the response of the VSG is more oscillatory compared to the droop-based techniques during system transients [16]. Also, the droop control suffers from its inherent drawbacks under large disturbances in the system. In [19] a generalized droop control is presented for supporting the grid. The power loop in this approach is adaptive to different conditions and enables the control system to provide virtual inertia and damping factor in standalone conditions. Moreover, in grid-connected mode, the fluctuations in the output power are reduced. Nevertheless, the drawbacks of tuning and designing optimal controller gains and droop coefficient could limit control functionalities especially if the network configuration is altered, or a large disturbance occurs.

Due to the high level of nonlinearity in PEDG and aforementioned shortcomings in the operational methodologies, it is worthy to mention that the conventional droop and VSG based controls have shortcomings to pick up the load for distinct dynamic characteristics either in grid-tied or standalone mode of operation at the same time. Whereas artificial intelligence (AI)-based techniques sound more attractive to address the challenges in enhancing resiliency and improving transient response in low inertia power systems [20]. AI techniques can cope up with multi-objective optimization problems such as frequency and voltage restorations. Moreover, AI can dynamically learn the demand of power during load or generation disturbances to rapidly restore the frequency of the system and prevents low frequency-nadirs and high ROCOFs. This will ultimately prevent the system from cascaded failures and blackouts, thus increasing the system resiliency. In fact, AI techniques are believed as a suitable potential to accommodate complicated dynamic modification of the system. Specifically, this feature of AI will help to improve the transient response in low-inertia power system such as PEDG.

Consequently, an AI-based frequency control is presented in [20] which focuses on an isolated hydro power plant. This methodology is valid for isolated plants where the required data are available for training. Therefore, the training process does not cover all the system incidents. Besides, any modification in the network configuration will have negative impacts on the

outcome of the offline trained network. Also, in [21-23], multi-agent reinforcement learning methods are explored to remove the centralized control approaches by estimating the frequency at primary and secondary levels. Still, the practical implementation of the proposed approaches is limited by the required communication infrastructure. Moreover, selecting a proper AI technique, as well as training and implementing methodologies for the targeted system are undeniable challenges.

This paper proposes an artificial intelligence-based power reference correction (AI-PRC) technique for GFLIs to autonomously adjust their power setpoints during transient disturbances. The proposed AI-PRC technique enables fast frequency restoration to enhance the transient response and resiliency of PEDG via re-defining GFLIs role at the grid-edge. The proposed AI-PRC technique includes a data mining mechanism and real-time AI-prediction module in the control loop of GFLI. The data mining approach is based on a comprehensive transient and steady state-based analytical model to construct a thorough database. All PEDG physical features such as practical alterations in configurations, demand and supply side disturbances, different inertia constants, network natural and damping frequency related to the power angle, and the optimal power injection/absorption are considered in this approach. All feasible variables are valued based on their practical ranges in a realistic PEDG. In this process, different parameters are considered such as inertia constant, alterations in grid configuration (i.e., the X/R ratio), demand and supply disturbances, system damping coefficient, natural frequency, and damped natural frequency. Thereafter, the required injecting/ absorbing power is calculated forthrightly. After that, a two-layer feedforward neural network with optimal number of sigmoid hidden neurons and linear output neuron is learned by using the mathematical-driven database. A Bayesian regularization algorithm (BRA) is employed in the training stage to compensate the dataset size limitations, mitigate the noisy dataset impact, and address the other potential uncertainties. The real-time AI-prediction module accurately predicts frequency trajectory when a transient disturbance occurs in the system. Thus, the proposed methodology scrutinizes frequency eccentricities during wide range of disturbances. The proposed methodology is employed in the control loop of GFLIs to ensure resilient operation of PEDG under disturbances. Thus, the main contribution of this paper is to address the shortcomings of frequency restoration among the state-of-the-art VSG-based or droop-based GFLIs and GFMIs via re-defining GFLI role at grid-edge equipped with the proposed AI-PRC.

The remainder of this paper is organized as follows: Section II provides a description of considered system and PEDG dynamic fundamentals. Section III discusses the proposed data mining methodology. Section IV details technical aspects of the training mechanism. In Section V, simulation and experimental validation are provided. Section VI concludes the paper.

II. PEDG Prevailing Dynamical Fundamentals

A. Considered System Overview

Fig. 1 represents the considered PEDG that is an IEEE 14-bus system. Seven GFLIs and one relatively small SG are contributing to support system loading. The total amount of load in this study is 500 kW. SG output power in steady state is limited to 150 kVA while its power rating is 800 kVA. As planned, 350 kW of system demand is supplied by renewable
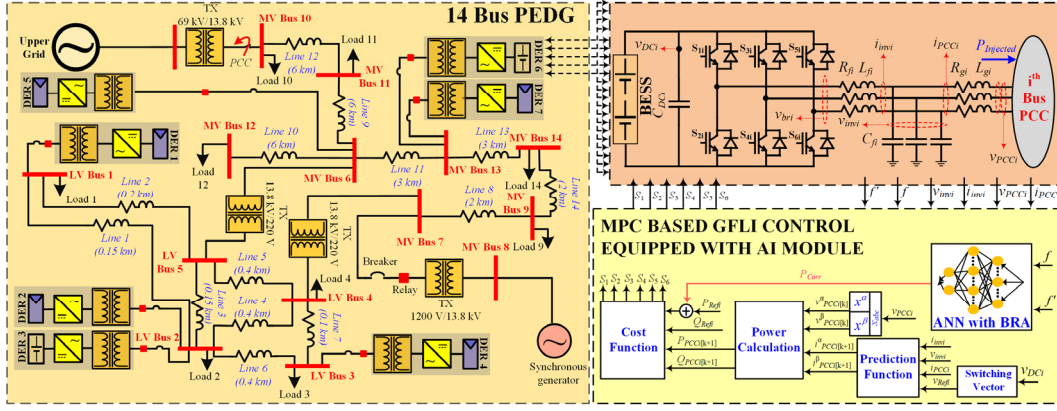
Fig. 1. The understudy 14-bus PEDG and control structure for i[th] GFLI equipped with AI module.

resources which is equivalent to 70% of the total system load, representing a highly renewable energy penetrated grid. The considered network has two voltage levels at 13.8 kV and 380 V. Furthermore, it can operate in islanded mode from upstream network at 69 kV via a circuit breaker installed at substation location of bus #10.

B. MPC based GFLI control

This section provides a brief overview of MPC formulation [24, 25] for GFLI control and switching signal generation. The GFLI is interfaced with LCL filter, thus the state-space representation of the continuous-time system shown in Fig. 1 is given as,

$$\frac{di}{dt}\begin{bmatrix} i_{inv,k}^{\alpha\beta} \\ v_{inv,k}^{\alpha\beta} \\ i_{pcc,k}^{\alpha\beta} \end{bmatrix} = A\begin{bmatrix} i_{inv,k}^{\alpha\beta} \\ v_{inv,k}^{\alpha\beta} \\ i_{pcc,k}^{\alpha\beta} \end{bmatrix} + B\left[v_{br,k}^{\alpha\beta} \right] + D\left[v_{pcc,k}^{\alpha\beta} \right] \tag{1}$$

where A, B, and D represent the system matrices as,

$$A = \begin{bmatrix} -R_f/L_f & -1/L_f & 0 \\ 1/C_f & 0 & -1/C_f \\ 0 & 1/L_g & -R_g/L_g \end{bmatrix} \quad B = \begin{bmatrix} 1/L_f \\ 0 \\ 0 \end{bmatrix} \quad D = \begin{bmatrix} 0 \\ 0 \\ -1/L_g \end{bmatrix}$$

The next step prediction is made by discretizing the given system in (1) with a step time of Ts. Hence, the state-space representation in discretized domain is given by,

$$\begin{bmatrix} i_{inv,k+1}^{\alpha\beta} \\ v_{inv,k+1}^{\alpha\beta} \\ i_{pcc,k+1}^{\alpha\beta} \end{bmatrix} = A_d\begin{bmatrix} i_{inv,k+1}^{\alpha\beta} \\ v_{inv,k+1}^{\alpha\beta} \\ i_{pcc,k+1}^{\alpha\beta} \end{bmatrix} + B_d\left[v_{br,k}^{\alpha\beta} \right] + D_d\left[v_{pcc,k}^{\alpha\beta} \right] \tag{2}$$

where matrices A_d, B_d and D_d are defined as,

$$A_d = e^{AT_s} \qquad B_d = A^{-1}(A_d - I_{3\times3})B \qquad D_d = A^{-1}(A_d - I_{3\times3})D$$

The next step prediction of active-reactive power is given by,

$$P_{k+1} = v_{pcc,k}^{\alpha} i_{inv,k+1}^{\alpha} + v_{o,k}^{\beta} i_{inv,k+1}^{\beta}$$
$$Q_{k+1} = v_{pcc,k}^{\beta} i_{inv,k+1}^{\alpha} - v_{pcc,k}^{\alpha} i_{inv,k+1}^{\beta} \tag{3}$$

The cost function subject to the minimization to generate the optimal switching signals for GFLI control is given by,

$$g_{GFL} = \left[\left(P_{ref,k} + P_{corr,k} \right) - P_{k+1} \right]^2 + \left[Q_{ref} - Q_{k+1} \right]^2$$
$$S_{z+1} = \arg\min(g_{GFL}) \tag{4}$$

where P_{ref} and Q_{ref} are the reference active and reactive power. To restore the frequency of PEDG under the disturbance, the AI module generates the corrective power P_{corr} that is used to

provide the active power reference for the MPC based GFLI controller. Furthermore, the reactive power reference can be set zero for unity power factor operation or as per system requirement. For the three-phase GFLI, there are 8 switching vectors and for each vector the cost function is calculated. The switching vector that represents the minimum value of the cost function is selected as the optimized vectors and the output of the MPC based voltage controller. Hence, based on this input from the AI, the MPC scheme tracks the active power reference to adjust active power injection to support the frequency.

C. PEDG Dynamic Fundamentals

In bulky power system with different rotational inertias, power balance equation defines the frequency trajectory of the system. That is based on the fundamental of swing equation which is valid for all SG-based power systems. As depicted in Fig. 1, in a typical PEDG, the power generation can be based on GFMIs, GFLIs, and small scale SGs. The fundamental swing equation is given as,

$$T_m - (T_e + D_a \Delta\omega_v) = 2H\frac{d\omega_v}{dt} \tag{5}$$

where H is the inertia constant, T_m is the mechanical torque of the prime-mover and T_e is defined as the torque that applied in reverse rotation due to the demand alterations. D_a is the damping factor and ω_v represents the system frequency. The primary effect of H is on the ROCOF while D_a has influence on the steady-state value of the frequency. To declare the legitimacy of this idea in mathematical form, one can simplify (5) by transferring torque equation in term of power balance at nominal frequency during load increase and ignoring the damping factor just at the disturbance instance. The ROCOF and accelerating power are given by,

$$\frac{df}{dt} = \frac{\Delta p}{2H}, \quad \Delta p = -\sqrt{-4H\Delta f\frac{dp_{gov}}{dt}} \tag{6}$$

where dp_{gov}/dt represent the governor dynamic. Mostly droop-based approaches are typically used in control schemes of GFLIs or GFMIs for voltage and frequency restoration [26]. In all droop-based controls, there is a basic relation between the frequency and the output active power given by,

$$f = \frac{D_p}{2\pi}\left(\frac{\omega_{cut}}{\omega_{cut}+s} \right)(p_0 - p) + f_0 \tag{7}$$

where f and f_0 are the frequency and its nominal value. p represents the output power of inverter and p_0 is the

nominal value of the active power. D_p is the droop coefficient and ω_{cut} is the low pass filter cut-off frequency. Due to the inherent alliance of inertia momentum with the inertia constant and incorporating the frequency governor dynamics, (5) can be represented in the term of power balance as,

$$p_{nom} - k_G(\omega - \omega_0) - (p_e + D_a(\omega_v - \omega_0)) = J\omega_0 \frac{d(\omega_v - \omega_0)}{dt} \quad (8)$$

where P_m can be represented as reference active power of inverter which in SGs is known as prime mover power, P_e is the inverter output power and ω_v is the output voltage angular frequency. k_G is known as governor gain. D_a and ω_0 are the damping factor and nominal system angular frequency respectively. Performing the Laplace transform on (8) and then, equating similar terms [27, 28] in (7) and (8) will result in,

$$J\omega_0 = \frac{1}{D_p \omega_{cut}} \;,\; k_G = \frac{1}{D_p} \quad (9)$$

This shows that the droop-based control can be equated as VSG-based control which follows the fundamentals of swing equation. Thus, it is proved that the prevailing dynamic of network of GFMIs and GFLIs, representing an islanded cluster of PEDG, follows the swing equation rule either they have VSG-based or droop-based control schemes. This fact, swing equation as the dominant dynamic response rule in PEDG, is used for initiating the data mining in this paper as detailed in the next section.

III.   PROPOSED DATA MINING METHODOLOGY

To provide a comprehensive dataset regarding feasible impending variations in the grid such as PEDG's physical feature or different disruption types, transient and steady-state intervals should be investigated accurately. The overall system resiliency cannot be achieved without considering both the steady state and transient stability. Thus, the data mining approach in this paper is based on both steady state and transient dynamics by analyzing and determining solutions of the swing equation as the dominant dynamic response rule in PEDG which is validated in the previous section.

A. Frequency dynamic in steady state condition

The steady state and transient dynamics of the PEDG is analyzed to provide a thorough database to cover primary and secondary frequency responses. These procedures assure that all events would be monitored and captured mathematically in a database that is exploited for learning a neural network. The final objective is to predict the PEDG frequency trajectory and provide an optimal power reference correction for GFLIs in real time. This real-time power correction is corresponding to the adjustment of accelerating power in conventional power systems by SGs contributions all over the grid. The intrinsic dynamics of PEDG during typical disturbances such as addition of load, loss of generation, etc. is evaluated by exploring the fundamentals of power balance equation,

$$f.(P_m - P_e) = \frac{H}{\pi}\left(\frac{d}{dt}\left(\frac{d\delta}{dt}\right)\right), \quad (10)$$
$$d\delta = \Delta w\, dt, P_e = P_M \sin(\delta)$$

where P_m is the per unit value of the inverters' input powers and P_e represents the output electrical power respectively. H is the virtual inertia constant, and δ is the electrical power angle. Any deviation in $\Delta\omega$ results in different frequency dynamic and ROCOF based on the PEDG inertia constant. For evaluating the inherent dynamic of this equation, a general perturbation such as $\delta = \Delta\delta + \delta_0$ is applied on the power angle, which is corresponded to a normal disturbance, (10) is approximated in term of angle perturbation by,

$$\left(\frac{d}{dt}\left(\frac{d\Delta\delta}{dt}\right)\right) = -\frac{\pi f}{H} P_M \cos(\delta_0)\Delta\delta \quad (11)$$

The effect of damping factor in inverter-based control loop can be demonstrated as $P_{dam} = D_a\, \Delta\omega$ that alters the electrical demand and thus the entire frequency dynamic during any potential disturbances. Thus, this impact can be considered in (11) which results in,

$$\left(\frac{d}{dt}\left(\frac{d\Delta\delta}{dt}\right)\right) = -\frac{D\pi f}{H}\frac{d\Delta\delta}{dt} - \frac{\pi f}{H} P_M \cos(\delta_0)\Delta\delta \quad (12)$$

By solving the characteristic equation, the power angle with respect to initial point of electrical power angle is given by,

$$\frac{\delta}{\delta_0} = 1 + \frac{\Delta\delta}{\delta_0\sqrt{1 - \left(\frac{D^2\pi f}{4H P_M \cos(\delta_0)}\right)}} e^{\frac{D\sqrt{\pi f}}{\sqrt{4H P_M \cos(\delta_0)}}\sqrt{\frac{\pi f}{H} P_M \cos(\delta_0)}\, t}$$
$$\sin\left(\sqrt{\frac{\pi f}{H} P_M \cos(\delta_0)\left(1 - \left(\frac{D^2\pi f}{4H P_M \cos(\delta_0)}\right)\right)}\, t + \theta\right) \quad (13)$$
$$\theta = \tan^{-1}\left(\frac{\sqrt{1 - \left(\frac{D^2\pi f}{4H P_M \cos(\delta_0)}\right)}}{\frac{D\sqrt{\pi f}}{\sqrt{4H P_M \cos(\delta_0)}}}\right)$$

Thus,

$$\omega_d = \sqrt{\frac{\pi f}{H} P_M \cos(\delta_0)\left(1 - \left(\frac{D^2\pi f}{4H P_M \cos(\delta_0)}\right)\right)}$$
$$\omega_n = \sqrt{\frac{\pi f}{H} P_M \cos(\delta_0)} \;,\; \xi = \frac{D\sqrt{\pi f}}{\sqrt{4H P_M \cos(\delta_0)}} \quad (14)$$

The natural and damped frequencies and damping ratio are extracted from (13) and given in (14). Therefore, PEDG as a nonlinear system has natural frequency which has influence on the nodal voltages, global frequency, and the amount of power contribution from each DER. Furthermore, natural frequency is affected reversely by H while the damping ratio has a direct relation with damping factor. As expected, by increasing the inertia constant, damping ratio of the PEDG is decreased. Thus, the generalized power angle equation can provide a comprehensive database for frequency and ROCOF dynamic if the input variables are valued in a feasible and practical range.

B. Transient frequency dynamic during severe disturbances

By contemplating potential severe disturbances and degree of nonlinearities in PEDG, the steady state frequency analysis would not be pertinent to assess the PEDG dynamic. In other words, when the disturbance is extensive, common, and straightforward solutions are not reasonable for a highly coupled nonlinear differential equation. The PEDG dynamic facing with a severe disturbance is obtained by using Euler arithmetical methodology. In this approach, some adjustments which are based on prediction and correction techniques are applied. Basically, (10) can be divided in two first-order differential equation as,

$$\frac{\Delta p\,\pi f}{H} = \frac{d\Delta w}{dt}, d\delta = \Delta w\, dt \quad (15)$$
$$\Delta p = P_m - P_e$$

The predicted solutions are found for each equation and denoted by subscript N. Also, a corrective action is carried out on the predicted values and shown by subscript c. At the state of $k+1$, the predicted values for power angle are given by,

$$\frac{d\delta}{dt}\Big|_{(\Delta w_{k+1}^N)} = \Delta w_{k+1}^N$$

$$\Delta w_{k+1}^N - \Delta w_k = \frac{dw}{dt}\Big|_{(\delta_k)}.(t_{k+1}-t_k) \qquad (16)$$

Similarly, the angular frequency deviation is given by,

$$\frac{d\Delta w}{dt}\Big|_{(\delta_{k+1}^N)} = \frac{\pi f}{H}((P_m - P_e)\big|_{\delta_{k+1}^N})$$

$$\delta_{k+1}^N - \delta_k = \frac{d\delta}{dt}\Big|_{(\Delta w_k)}.(t_{k+1}-t_k), \qquad (17)$$

The corrected values are calculated by averaging the values of two found derivatives and is given by,

$$(\delta_{k+1}^c - \delta_k) = \frac{\frac{d\delta}{dt}\big|_{(\Delta w_k)}.(t_{k+1}-t_k) + \frac{d\delta}{dt}\big|_{(\Delta w_{k+1}^N)}.(t_{k+1}-t_k)}{2},$$

$$(\Delta w_{k+1}^c - \Delta w_k) = \frac{\frac{dw}{dt}\big|_{(\delta_k)}.(t_{k+1}-t_k) + \frac{dw}{dt}\big|_{\delta_{k+1}^N}.(t_{k+1}-t_k)}{2} \qquad (18)$$

For the next step, corrected values are substituted in associated equations and the process is repeated to find the last approximated solution for the objective states as,

$$\delta_{k+1}^c - \delta_{k+1} \cong 0, \ \Delta\omega_{k+1}^c - \Delta\omega_{k+1} \cong 0 \qquad (19)$$

Similarly, by finding the angle dynamic, frequency and ROCOF are found considering different grid features such as inertia constant, damping factor and the supply-demand disturbances.

IV. PROPOSED TRAINING MECHANISM

A. AI Training description

Once a comprehensive dataset is formed, an artificial neural network (ANN) is needed to be trained for predicting the required corrective accelerating power to support the grid under different disturbances. The trained network, predict PEDG inertia based on the frequency trajectory and ROCOF and find an optimal power to restore frequency excursion in a timely manner. Typically, AI-based approaches suffer from lack of required database size, non-optimal regularization parameters, heterogenous datasets, overfitting problems and potential uncertain inputs. Using Bayesian regularization in the learning algorithm of ANN, enhances the training performance by finding the optimal parameters during training process. In BRA, defining a cost function is required to adaptively decide on terminating the training process based on different problem objectives and regularization parameters. A typical problematic issue in feed forward neural networks (NN) is regarded to overfitting challenges that have direct influence on the network weights. This results in poor neural network generalization when they get new input data. The best method to resolve this issue is to regularize the estimation process. This is carried out by inflicting a penalty factor on the network cost function. Based on the problem objective in this work, the inputs are system frequency and ROCOF while target dataset includes the required corrective active power to stabilize the PEDG under applied disturbances. Training datasets are given by,

$$T_d = \left\{ \left((f_1,f_1'),P_{corr1}\right), \left((f_2,f_2'),P_{corr2}\right),....,\left((f_N,f_N'),P_{corrN}\right) \right\} \qquad (20)$$

where f, f' are frequency and ROCOF and P_{corr} is the required corrective active power. A nonlinear mapping mechanism to represent the input-output relation can be obtained via a proper interpolating function. The mapping function is given by,

$$MP_i = \sum_{r=1}^{l} w_r \Psi_r(X_i) + G_i \ , \ X_i = (f_i, f_i'), MP_i = P_{corr,i} \qquad (21)$$

where $\psi(X_i)$ is defined as interpolating function with the weight factor w_r. G_i is a Gaussian random variable. The probability density function can be shaped in a general form needed for the optimization problem. In the proposed trajectory prediction process, it is aimed to minimize the prediction error given by,

$$E_{T_d} = \frac{1}{N}\sum_{i=1}^{N} \left(MP_i - \hat{MP}_i\right) \qquad (22)$$

where $\widehat{MP}_i$ is the predicted value which is the output of the trained ANN. A Hessian matrix is estimated by Levenberg-Marquardt algorithm for a given function $g: \mathbb{R}^n \to \mathbb{R}$ as,

$$H_g = \begin{bmatrix} \frac{\partial^2 g}{\partial x^2_1} & \frac{\partial^2 g}{\partial x_1 \partial x_2} & \cdots & \frac{\partial^2 g}{\partial x_1 \partial x_n} \\ \frac{\partial^2 g}{\partial x_2 \partial x_1} & \frac{\partial^2 g}{\partial x^2_1} & \cdots & \frac{\partial^2 g}{\partial x_2 \partial x_n} \\ \vdots & & & \\ \frac{\partial^2 g}{\partial x_n \partial x_1} & \frac{\partial^2 g}{\partial x_n \partial x_2} & \cdots & \frac{\partial^2 g}{\partial x^2_n} \end{bmatrix}_{n \times n} \qquad (23)$$

a second-order partial derivative for all pairs of variables in domain of g, shapes matrix elements. This matrix is used in AI algorithms for finding the saddle points and extremum of the given function. An objective cost function is defined by,

$$E_{r_d} = \eta \sum_{h=1}^{l} \sum_{p,q=1}^{m} (w_{pq}^h)^2 + \frac{(1-\eta)}{N}\sum_{i=1}^{N} \left(MP_i - \widehat{MP}_i\right) \qquad (24)$$

This cost function is used to maintain the generalization performance of the NN and η is defined as the weight factor of regularization with the value of $0 < \eta < 1$. In this stage, two different parameters are defined for the later objective function and (24) is reformed by,

$$F_{reg_d} = \rho E_{reg_d} + \mu E_{T_d}$$

$$E_{reg_d} = \sum_{h=1}^{l} \sum_{p,q=1}^{m} (w_{pq}^h)^2, E_{T_d} = \frac{1}{N}\sum_{i=1}^{N} \left(MP_i - \widehat{MP}_i\right) \qquad (25)$$

Based on the BRA fundamentals, the NN weight factors are selected in a random manner. Thus, probability function of NN's weights is given by,

$$f(w|T_d,\rho,\mu,N_n) = \frac{f(T_d|w,\mu,N_n)f(w|\rho,N_n)}{f(T_d|\rho,\mu,N_n)} \qquad (26)$$

In this equation, network model is involved and represented by N_n. Also, the initial information regarding the weight factors is identified as a prior density function of $f(w|\rho,N_n)$. Considering given weight factors, the probability of receiving the data T_d is shown by $f(T_d|w,\mu,N_n)$. Also, based on the probability fundamentals, a normalization term as $f(T_d|\rho,\mu,N_n)$ is used to ensure the total probability of 1 in (26). $f(T_d|w,\mu,N_n)$ by considering the Gaussian random variable with variance σ^2 in the mapping function can be found by,

$$f(T_d|w,\mu,N_n) = \frac{e^{-\frac{\mu}{N}\sum_{i=1}^{N}(MP_i - \widehat{MP}_i)}}{\sqrt{(2\pi\sigma^2)^N}} \qquad (27)$$

With the same approach,

$$f(w|\rho,N_n) = \frac{e^{-\rho\sum_{h=1}^{l}\sum_{p,q=1}^{m}(w_{pq}^h)^2}}{\int e^{-\rho\sum_{h=1}^{l}\sum_{p,q=1}^{m}(w_{pq}^h)^2} dw} \qquad (28)$$

Considering (27) and (28), (26) can be represented as,

$$f(w|T_d, \rho, \mu, N_n) = \frac{e^{-(\frac{\mu}{N}\sum_{i=1}^{N}(MP_i - \widehat{MP_i}) + \rho\sum_{h=1}^{l}\sum_{p,q=1}^{m}(w_{pq}^h)^2)}}{\int e^{-\rho\sum_{h=1}^{l}\sum_{p,q=1}^{m}(w_{pq}^h)^2} dw \sqrt{(2\pi\sigma^2)^N}} \quad (29)$$

By rearranging (26), the normalization term is given by,

$$f(T_d|\rho, \mu, N_n) = \frac{e^{-(\frac{\mu}{N}\sum_{i=1}^{N}(MP_i - \widehat{MP_i}) + \rho\sum_{h=1}^{l}\sum_{p,q=1}^{m}(w_{pq}^h)^2)}}{\left(\int e^{-\rho\sum_{h=1}^{l}\sum_{p,q=1}^{m}(w_{pq}^h)^2} dw\right)^2 (2\pi\sigma^2)^N} \quad (30)$$

(30) is estimated around the minimum point of w_m. Thus, to find the optimum point, derivative of (30) with respect to ρ, μ should be equal to zero. By applying Hessian matrix in optimization process, the optimum parameters are given by,

$$\rho_{op} = \eta(2\sum_{h=1}^{l}\sum_{p,q=1}^{m}(w_{pq}^h)^2 |w_m|^{-1}$$
$$\mu_{op} = (N - \eta)(\frac{2}{N}\sum_{i=1}^{N}(MP_i - \widehat{MP_i})|w_m|^{-1} \quad (31)$$

Getting the optimum parameters based on the training dataset structure, ensures high prediction accuracy of the trained network while enable the network to deal with noisy and small datasets with uncertain dynamic of inputs.

B. AI Training process

The ANN training requires about 1000 epochs using BRA as discussed in section IV-A. This algorithm typically requires lesser memory than the other techniques however at the cost of longer training times. Training automatically stops when generalization stops improving, as indicated by a decrease in the mean squared error (MSE) measure of the validation samples. As mentioned previously, frequency and ROCOF for different scenarios are used as inputs in the (12) and (15) to determine the accelerating power P_{corr} required. The solutions of (12) and (15) for different f_g and ROCOF inputs are used to generate a database as given by (20) that is fed as training data to the ANN. These design considerations make the trained ANN quick and robust in determining the accelerating power required. The MSE plotted in Fig. 2 is used as the merit to validate the performance accuracy of the trained ANN. As evident, after completion of the training process the MSE approaches zero.

The database is divided randomly so that training process uses 70%, testing uses 15% and validation uses 15% of the data. Furthermore, the selection of number of hidden layer neurons is based on a trade-off between the ANN's response time and accuracy. This value is specific to the system and is optimized to two hidden layers with 11 neurons in first hidden layer and two neurons in the second layer. An error histogram is plotted in Fig. 3 to show the performance obtained with the developed ANN. Finally, about 150,000 sample data are fed as input and target datasets to train the network.

V. Case Studies and Validation

The functionality of the proposed AI-based technique for enhancing the transient response and resiliency of PEDG is validated on two main setups: (i) an IEEE 14-bus network shown in Fig. 1 that represents a realistic PEDG in MATLAB/Simulink environment, (ii) a small-scale experimental hardware setup emulating the characteristics of
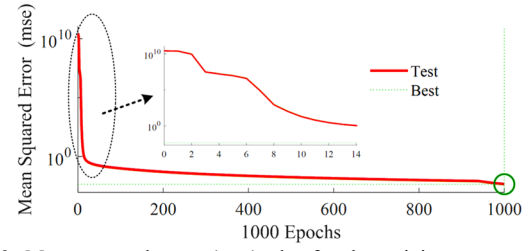

Fig. 2. Mean squared error (mse) plot for the training process of the proposed ANN.
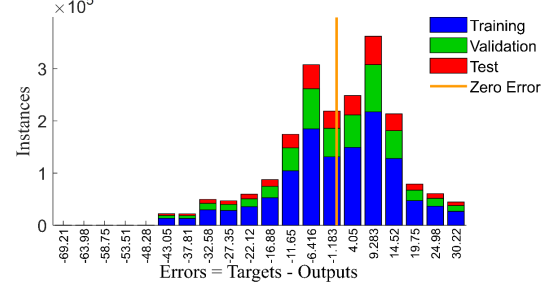

Fig. 3. Error histogram of the trained ANN.

PEDG. Specifically, the experimental hardware setup has two DERs, that are controlled as GFMI and GFLI feeding their local loads of 22 Ω and 30 Ω respectively. The interconnection between GFMI and GFLI is established via a line impedance.

A. Simulation Case Studies – 14-Bus Network

Several cases studies are simulated and assessed: *i*) extensive power generation loss in the grid due to potential external grid disturbances, *ii*) generation loss in a reconfigured grid topology, *iii*) load decrease in the reconfigured grid, *iv*) comparative case study of the proposed AI-PRC with state-of-the-art VSG and reverse droop-based control schemes for frequency restoration, *v*) robustness to model parameter mismatch. Furthermore, all case studies, thorough comparisons are presented with and without the proposed approach in PEDG.

Case Study I: In this scenario, the 14-bus PEDG's DERs are driving the total load during steady state. GFLIs are feeding the loads based on their pre-defined power set points. For evaluating the efficacy of the proposed AI-PRC based frequency restoration methodology, one of the GFLIs is equipped with the proposed AI-PRC. In case study I, a 200 kW generation loss occurs on PEDG when all DERs are unequipped with the AI-PRC. As expected, a considerable frequency drop is detected at the time of transient disturbance. Generation loss transpired at instant of t = 8 s. Fig. 4 (a) illustrates the grid's frequency before and after this disturbance in the considered system without and with the AI-PRC module enabled. As shown, in the system without AI, a frequency drop of 3 Hz is observed in red plot. In this scenario, SG is the main contributor to governing the voltage and frequency particularly in the black start and during grid potential disturbances. Here, frequency is restored by the SG's governor at the nominal value after 4 s. Moreover, the nadir frequency drops below 57 Hz which most probably triggers the protection relays. Comparatively, when the GFLI#6 is equipped with the proposed AI-PRC and during the event of loss of generation, as shown in Fig. 4 (a), the frequency is restored in timely manner indicated by blue plot. Considering the training mechanism, the power correction value is increased to 200 kW which shows the accuracy of the proposed AI-PRC. At the same time, SG is increasing the output power gradually due to its slower dynamic response. As SG power increases, the
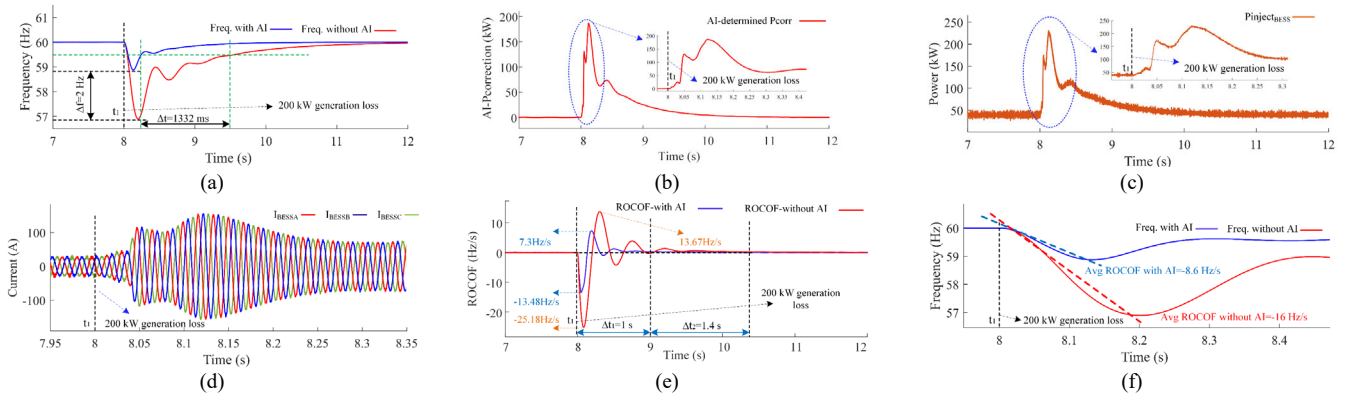
Fig. 4. Case Study I illustrating 14-bus PEDG under 200 kW generation loss: (a) frequency dynamic without and with proposed AI-PRC in GFLI#6, (b) AI-PRC determined P_{corr} before and after 200 kW generation loss, (c) power injection by GFLI#6, (d) output current dynamic of GFLI#6 (e) instantaneous ROCOF with and without proposed AI-PRC, and (f) zoomed view of frequency without and with proposed AI-PRC.

AI-PRC adjusts the power reference setpoint of the GFLI accordingly to its default value in about 4 s. Comparatively with AI-PRC module, the nadir frequency has improved by 2 Hz and the time required for frequency restoration is decreased by about 1332 ms when the GFLI supports the grid during transients. Fig. 4 (b) shows the correction value of active power that should be added to the power set point of GFLI to support the frequency during the transients. Moreover, Fig. 4 (c) shows the dynamic of active power injected via AI-PRC equipped GFLI#6 and this accurately follows its reference. Fig. 4 (d) illustrates the output current dynamics of GFLI#6 during the occurred disturbance. Similar to the corrected power reference, the current increases in three stages and converge to its nominal value after the disturbance is damped. Fig. 4 (e) provides exhaustive information regarding instantaneous ROCOF for with and without AI-PRC frequency restoration scenarios. As indicated, the maximum ROCOF is 13.48 Hz/s when the AI-PRC is deployed in the control loop of GFLI. This value reaches 25.18 Hz/s when GFLI does not contribute to frequency restoration. Fig. 4 (f) demonstrates that the average ROCOF improves approximately twice the time the AI-PRC approach is not employed in the GFLI's control loops. As indicated, the maximum average ROCOF is -8.6 Hz/s when the AI-PRC is deployed in the control loop of GFLI. This value reaches -16 Hz/s when GFLI does not contribute to frequency restoration.

Case Study II: To generalize the functionality of the proposed approach in grid support during severe transient disturbances, the grid structure is reconfigured and the limitation of the GFLI power rating is considered during their frequency restoration contribution in this case study. This physical variation would have explicit impact on the *X/R* ratio of the grid and the short circuit ratio (SCR). Both can affect the dynamic response of the grid during severe disturbances. The scenario provided in this case study thus validates that the trained neural network is well generalized and can predict the frequency trajectory when the physically modified understudy grid is confronted with severe transient disturbances. As shown in Fig. 1, two different transmission lines located in critical points of two different voltage level clusters committed to be disconnected. The employed modification alters the basic power flow paths remarkably. Assuming the power ratings are not jeopardized in this scenario after reconfiguration, a 120-kW power generation loss occurs in the understudy 14-bus network. Here, the GFLI at bus 13 will support the grid in transients. This DER has a power rating of 80 kW. Based on the local load of 50
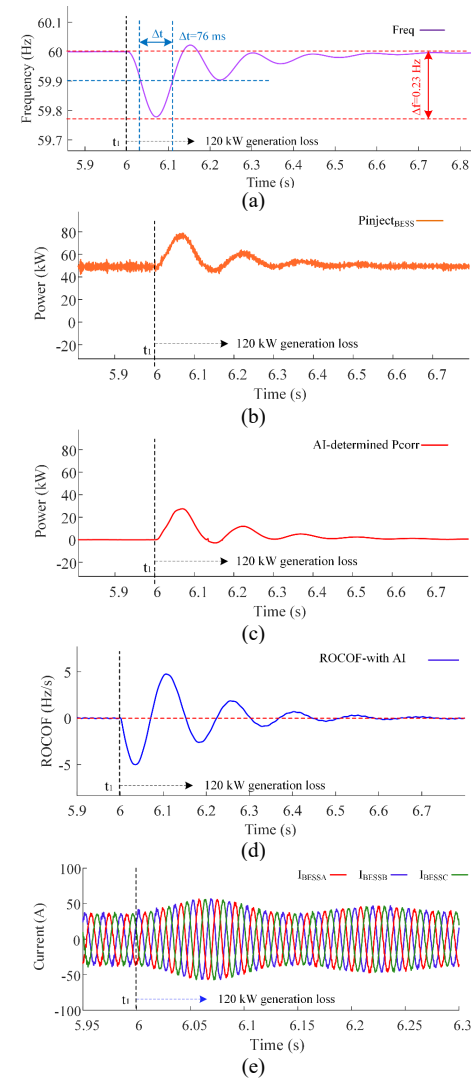

Fig. 5. Case Study II illustrating PEDG under 120 kW generation loss and network reconfiguration: (a) frequency dynamics, (b) power injected by GFLI#6, (c) AI-PRC determined P_{corr}, (d) instantaneous ROCOF, (e) GFLI#6 output current dynamics.

kW of this DER, the maximum power contribution of this DER is confined to 30 kW. Line 14 was being operated at MV voltage level and line 4 was at LV level. As a result, it is anticipated that the power flow in the line 11 increases due to the power
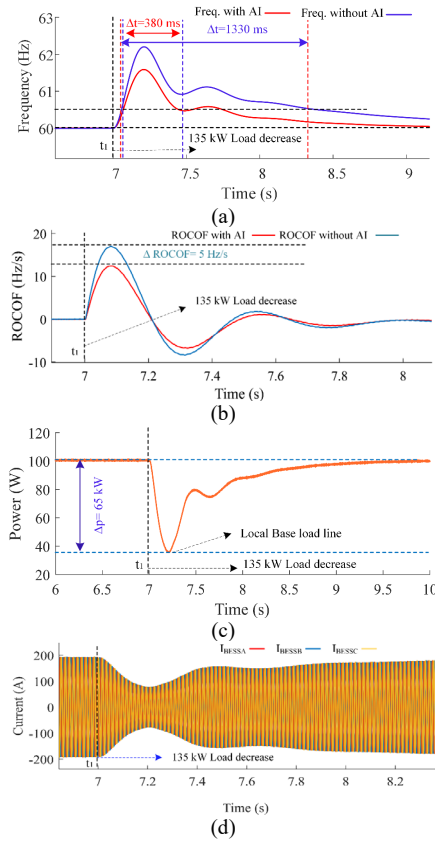
Fig. 6. Case Study III illustrating unplanned demand outage with a reconfigured grid and modified total inertia to demonstrate the performance of the proposed AI-PRC under different parameter variation: (a) frequency dynamics, (b) instantaneous ROCOF, (c) power injected by GFLI#3, (d) GFLI#3 output current dynamics.
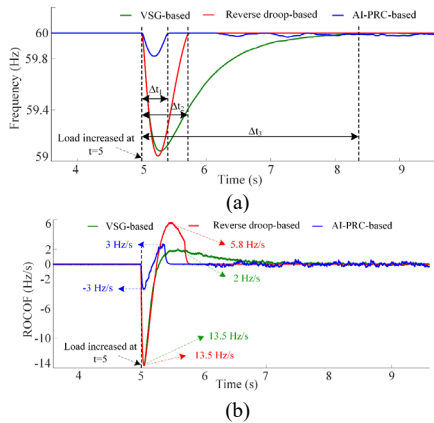

Fig. 7. Case Study IV illustrating comparison between proposed AI-PRC and state-of-the-art frequency restoration schemes (VSG and reverse-droop based schemes) with respect to (a) frequency dynamics, (b) ROCOF.

contribution from GFLI#6. Fig. 5 (a) illustrates the frequency excursion dynamic before and after this disturbance. As shown, the frequency is restored beyond 59.9 Hz around 76 ms while the frequency nadir differences with nominal value is kept in the band of 0.23 Hz. Fig. 5 (b) shows the power contribution of the GFLI during the transient by following the power correction AI-PRC's command shown in Fig. 5 (c). As shown, the maximum power contribution is around 20-30 kW to go along with the power rating restriction. The ROCOF during the transients is in an acceptable range as depicted in Fig. 5 (d). The current
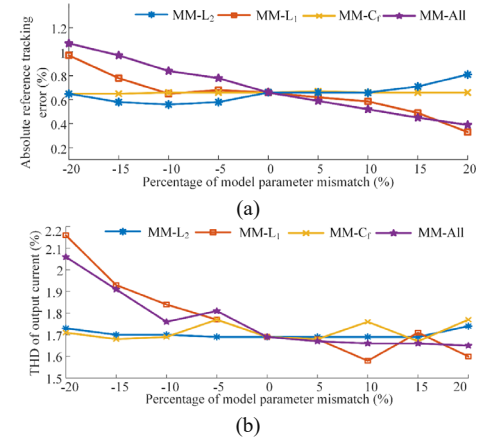

Fig. 8. Case Study V illustrating robustness of the proposed AI-PRC to model parameter mismatch that uses MPC for switching sequence generation: (a) active power reference tracking error with mismatch (MM) in the parameters from the actual value, (b) Total harmonic distortion (THD) of the GFLI output current with mismatch in the parameters from the actual value.

dynamic of this inverter is illustrated in Fig 5 (e). As shown, the current increases based on the dynamic change of power reference. Hence, this case study highlights the effective contribution of GFLIs in frequency restoration even by considering inverter power rating limitations and grid reconfiguration scenario.

Case Study III: this case study analyzes the impact of an unplanned demand outage. At instant t = 7 s, 135 kW load is decreased. The grid is reconfigured, the location of the supportive GFLI is changed (located at bus#2) and the total inertia of the grid is modified. Although the entire inertia of the grid is an unknown parameter, by modifying the SG's inertia constant, total grid inertia would be affected, and this case study can be an operational assessment of the trained neural network in the frequency trajectory prediction practice. As expected, the AI module ought to deliver a negative power reference to adjust the GFLI power reference in a way that power injection to the grid decreases although the inverter should sustain its local load of 35 kW. In a steady state, the power injection was around 100 kW when the unplanned demand outage occurred. Frequency and ROCOF dynamics are captured and assessed in Fig. 6 (a) and (b) correspondingly. In more detail, a comparison of frequency dynamics with and without deploying the AI-PRC in GFLI control loops for the similar disturbance is shown by red and blue plots respectively. As shown, frequency is controlled lower than 60.5 Hz in 380ms. The frequency peak is suppressed considerably when deploying the proposed approach. A considerable improvement in ROCOF of 5 Hz/s is observed by deploying the proposed AI-PRC (see Fig. 6 (b)). Fig. 6 (c) shows the power dynamic of the GFLI. As expected, the injected power is decreased and reached to a new level while the predefined constraints of inverter local load power is not jeopardized. The disturbance is restrained by 2.5 s during the time that SG declines its output power to make up a new supply-demand. Fig. 6 (d) shows the inverter current dynamics during the grid support. The current gets the minimum acceptable value by 200 ms to dampen the disturbance and raises to the nominal value after about 130 ms.

Case Study IV: In this case study, we consider a network of a GFMI and a GFLI that are connected as shown in Fig. 9 (b).
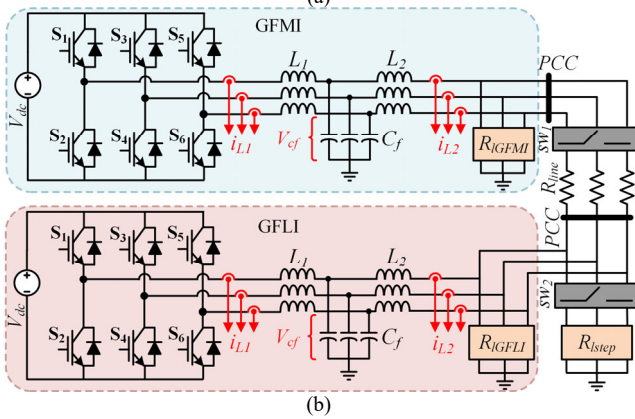
Fig. 9. (a) Hardware setup for experimental validation of the proposed AI-PRC scheme, (b) connection schematic between GFMI and GFLI in the hardware testbed.

TABLE. I: SYSTEM SPECIFICATIONS

Parameter	Value & units
Dc link voltage V_{dc}	300 V
Sampling time T_s	25 μs
Inverter side inductance L_1	3.06 mH
Grid side inductance L_2	1.364 mH
Filter capacitor C_f	24.69 μF
Peak voltage V_g	150 V
Grid Frequency f_g	60 Hz
GFMI and GFLI rated power	5000 W
GFMI local load	30 Ω
GFLI local load	22 Ω
Step Load	20 Ω

This case study compares the transient response of frequency for three different frequency restoration schemes: VSG, droop-based, and the proposed AI-PRC scheme. Fig. 7 (a) represents the frequency response obtained from the various compared GFLI control schemes in response to a load step change of 100%. The results show that the network experiences the least frequency deviation with the value of 0.15 Hz (blue plot) when equipped with the proposed AI-PRC while the frequency deviations observed for other methods are 0.85 Hz (green plot for VSG-based control scheme) and 0.9 Hz (red plot for reverse droop-based control scheme). It is worth mentioning that the frequency restoration times required for each method are 3 s (for VSG-based), 0.6 s (reverse droop-based), and 0.4 s (for proposed AI-PRC). These results indicate the superiority of the proposed AI-PRC scheme in terms of minimum restoration
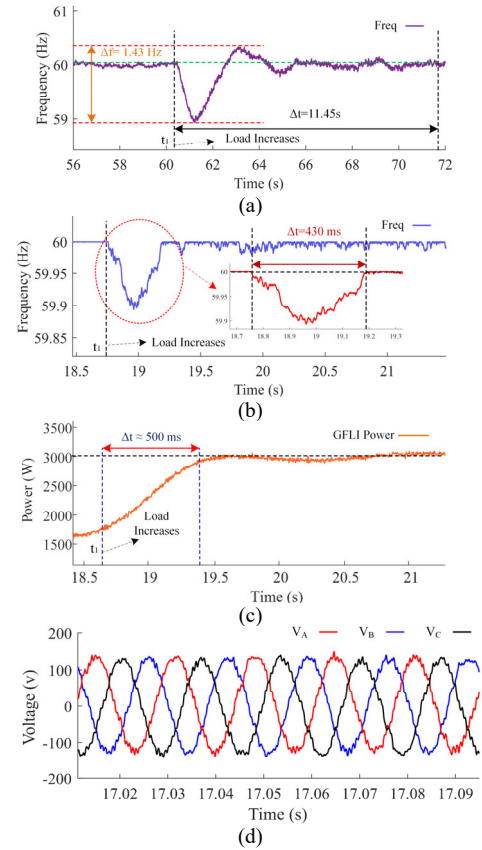

Fig. 10. Results for Case Study V illustrating experimental validation of proposed AI-PRC frequency restoration scheme: (a) frequency dynamics without AI-PRC (VSG based frequency restoration), (b) frequency dynamics with proposed AI-PRC, (c) power injected by GFLI with AI-PRC for frequency restoration, (d) PCC voltage profile.

time and frequency deviation. Furthermore, Fig. 7 (b) provides the ROCOF comparison for each method. As observed, the proposed method provides the least ROCOF of 3 Hz/s (blue plot) in contrast to the ROCOF of 13.5 Hz/s obtained for the other two control schemes (green and red plots).

Case study V: In this case study, the impact of model parameter mismatch on the practicality and capability of the proposed AI-PRC which uses an MPC-based modulator to generate the switching sequences is studied. The absolute reference tracking error of the active power for the introduced mismatch of ±20 % in the values of L_1, L_2, and C_f is represented in Fig. 8 (a). Total harmonic distortion (THD) of the output current of the GFLI with the proposed AI-PRC under the same mismatch is also depicted in Fig. 8 (b). As it is shown in this case study, the proposed AI-PRC is robust to model parameter mismatch.

B. Experimental Case Studies

The functionality of the proposed AI-PRC scheme is also validated experimentally on a small-scale hardware setup depicted in Fig. 9 (a). The schematic diagram of the connection between GFMI and GFLI is illustrated in Fig. 9 (b). The understudy hardware emulates a realistic dynamic of a network of GFMI and GFLIs islanded cluster. Thus, voltage and frequency are built and controlled via a relatively low-inertia VSG-based GFMI. Also, a GFLI contributes to support the local load. The specifications of the hardware components are

listed in Table. I. The GFLI and GFMI controllers are implemented in dSPACE Microlabox.

Case Study VI: In this case study, the superiority of the proposed AI-PRC approach is validated. In the first scenario, the frequency restoration is performed by the governor (conventional PI-based) control loop of the VSG based GFMI while in the second scenario the GFLI is equipped with the AI-PRC module to support restoring the frequency during the load disturbance. Specifically, a step load of around 1500 W is applied on the grid. Fig. 10 (a) illustrates the frequency dynamics with VSG based frequency restoration scheme. As shown, the system frequency is restored to the nominal value. However, the restoration time is around 11.45 s in this low inertia grid, and this is due to the drawbacks of PI-based control approaches. High proportional and integral gains can enhance the restoration time, but those cannot be employed in practice. Indeed, if a severe load disturbance occurs, the frequency drop will push the protection relays to be triggered instantaneously. Comparatively in the second scenario when GFLI is equipped with the AI-PRC module for the frequency restoration support, Fig. 10 (b) demonstrates system frequency dynamics. As shown, the frequency is restored to the nominal value of 60 Hz within 430 ms which is about 26 times faster as compared to the VSG approach, considering the severity of the disturbance. Furthermore, Fig. 10 (c) illustrate the output power dynamics of GFLI with the proposed AI-PRC. The system supports the extra load of 1.5 kW within 500 ms. Finally, the Fig. 10 (d) shows the PCC voltage profile. Thus, the effectiveness of proposed scheme is validated experimentally. This case study shows the importance of re-defining the GFLI's role at grid-edge in handling transient disturbances.

VI. CONCLUSION

This paper proposes re-defining the role of GFLIs at the grid-edge via an AI-PRC mechanism to enhance the transient response and resiliency of PEDG. A two-layer feedforward ANN is learned by the Bayesian regularization algorithm which facilitates the AI-PRC module to predict system frequency trajectory and provide the proper amount of correction power for GFLIs when the grid is subjected to disturbances. GFLI and GFMI dynamic is extensively analyzed to create an accurate data mining approach for the training of the ANN. Several simulation and experimental case studies are provided that demonstrate significant improvement in transient response and resiliency in comparison with state-of-the-art frequency restoration mechanism.

ACKNOWLEDGMENT

REFERENCES

[1]   A. Khan, M. Hosseinzadehtaher, M. B. Shadmand, S. Bayhan, and H. Abu-Rub, "On the Stability of the Power Electronics-Dominated Grid: A New Energy Paradigm," *IEEE Industrial Electronics Magazine,* vol. 14, no. 4, pp. 65-78, 2020, doi: 10.1109/MIE.2020.3002523.

[2]   Q. Peng, Q. Jiang, Y. Yang, T. Liu, H. Wang, and F. Blaabjerg, "On the Stability of Power Electronics-Dominated Systems: Challenges and Potential Solutions," *IEEE Transactions on Industry Applications,* vol. 55, no. 6, pp. 7657-7670, 2019, doi: 10.1109/TIA.2019.2936788.

[3]   U. Markovic, O. Stanojev, P. Aristidou, E. Vrettos, D. Callaway, and G. Hug, "Understanding Small-Signal Stability of Low-Inertia Systems," *IEEE Transactions on Power Systems,* vol. 36, no. 5, pp. 3997-4017, 2021, doi: 10.1109/TPWRS.2021.3061434.

[4]   L. Meegahapola, P. Mancarella, D. Flynn, and R. Moreno, "Power system stability in the transition to a low carbon grid: A techno-economic perspective on challenges and opportunities," *WIREs Energy and Environment,* vol. 10, no. 5, p. e399, 2021.

[5]   G. Yuan, "Grid-Forming Technologies Enabling a Decarbonized Power System [Technology Leaders]," *IEEE Electrification Magazine,* vol. 10, no. 1, pp. 7-9, 2022, doi: 10.1109/MELE.2021.3139204.

[6]   Y. Lin *et al.*, "Research Roadmap on Grid-Forming Inverters," United States, 2020-11-11 2020.

[7]   R. Rosso, X. Wang, M. Liserre, X. Lu, and S. Engelken, "Grid-forming converters: an overview of control approaches and future trends," in *2020 IEEE Energy Conversion Congress and Exposition (ECCE),* 11-15 Oct. 2020 2020, pp. 4292-4299, doi: 10.1109/ECCE44975.2020.9236211.

[8]   E. A. A. Coelho, P. C. Cortizo, and P. F. D. Garcia, "Small-signal stability for parallel-connected inverters in stand-alone AC supply systems," *IEEE Transactions on Industry Applications,* vol. 38, no. 2, pp. 533-542, 2002, doi: 10.1109/28.993176.

[9]   B. K. Poolla, D. Groß, and F. Dörfler, "Placement and Implementation of Grid-Forming and Grid-Following Virtual Inertia and Fast Frequency Response," *IEEE Transactions on Power Systems,* vol. 34, no. 4, pp. 3035-3046, 2019, doi: 10.1109/TPWRS.2019.2892120.

[10] S. D'silva, M. Hosseinzadehtaher, M. B. Shadmand, S. Bayhan, H. Abu-Rub, and T. Huang, "Coordinated Power Reserve Control of PV Sources For Frequency Restoration in Power Electronics Dominated Grid," in *2022 3rd International Conference on Smart Grid and Renewable Energy (SGRE),* 2022: IEEE, pp. 1-7.

[11] V. Gevorgian, "Highly accurate method for real-time active power reserve estimation for utility-scale photovoltaic power plants," National Renewable Energy Lab.(NREL), Golden, CO (United States), 2019.

[12] A. Khan, S. D. silva, A. Y. Fard, M. B. Shadmand, and H. Abu-Rub, "On Stability of PV Clusters With Distributed Power Reserve Capability," *IEEE Transactions on Industrial Electronics,* vol. 68, no. 5, pp. 3928-3938, 2021, doi: 10.1109/TIE.2020.2987291.

[13] Q. C. Zhong and G. Weiss, "Synchronverters: Inverters That Mimic Synchronous Generators," *IEEE Transactions on Industrial Electronics,* vol. 58, no. 4, pp. 1259-1267, 2011, doi: 10.1109/TIE.2010.2048839.

[14] V. Karapanos, P. Kotsampopoulos, and N. Hatziargyriou, "Performance of the linear and binary algorithm of virtual synchronous generators for the emulation of rotational inertia," *Electric Power Systems Research,* vol. 123, pp. 119-127, 2015.

[15] Á. Ortega and F. Milano, "Combined Frequency and RoCoF Control of Converter-Interfaced Energy Storage Systems," *IFAC-PapersOnLine,* vol. 52, no. 4, pp. 240-245, 2019.

[16] J. Liu, Y. Miura, and T. Ise, "Comparison of Dynamic Characteristics Between Virtual Synchronous Generator and Droop Control in Inverter-Based Distributed Generators," *IEEE Transactions on Power Electronics,* vol. 31, no. 5, pp. 3600-3611, 2016, doi: 10.1109/TPEL.2015.2465852.

[17] D. Sun, H. Liu, S. Gao, L. Wu, P. Song, and X. Wang, "Comparison of Different Virtual Inertia Control Methods for Inverter-based Generators," *Journal of Modern Power Systems and Clean Energy,* vol. 8, no. 4, pp. 768-777, 2020, doi: 10.35833/MPCE.2019.000330.

[18] U. Tamrakar, D. Shrestha, M. Maharjan, B. P. Bhattarai, T. M. Hansen, and R. Tonkoski, "Virtual Inertia: Current Trends and Future Directions," *Applied Sciences,* vol. 7, no. 7, doi: 10.3390/app7070654.

[19] X. Meng, J. Liu, and Z. Liu, "A Generalized Droop Control for Grid-Supporting Inverter Based on Comparison Between Traditional Droop Control and Virtual Synchronous Generator Control," *IEEE Transactions on Power Electronics,* vol. 34, no. 6, pp. 5416-5438, 2019.

[20] S. Syan and G. R. Biswal, "Frequency control of an isolated hydro power plant using artificial intelligence," in *2015 IEEE Workshop on Computational Intelligence: Theories, Applications and Future Directions (WCI),* 14-17 Dec. 2015 2015, pp. 1-5.

[21] Z. Yan and Y. Xu, "A Multi-Agent Deep Reinforcement Learning Method for Cooperative Load Frequency Control of a Multi-Area Power System," *IEEE Transactions on Power Systems,* vol. 35, no. 6, pp. 4599-4608, 2020, doi: 10.1109/TPWRS.2020.2999890.

[22] Y. Liang, X. Zhao, and L. Sun, "A Multi-Agent Reinforcement Learning Approach for Wind Farm Frequency Control," *IEEE Transactions on Industrial Informatics,* pp. 1-10, 2022, doi: 10.1109/TII.2022.3182328.

[23] S. Rozada, D. Apostolopoulou, and E. Alonso, "Load Frequency Control: A Deep Multi-Agent Reinforcement Learning Approach," in *2020 IEEE Power & Energy Society General Meeting (PESGM)*, 2-6 Aug. 2020 2020, pp. 1-5, doi: 10.1109/PESGM41954.2020.9281614.

[24] S. Vazquez *et al.*, "Model predictive control: A review of its applications in power electronics," *IEEE industrial electronics magazine,* vol. 8, no. 1, pp. 16-31, 2014.

[25] M. F. Umar *et al.*, "Single-Phase Grid-Interactive Inverter With Resonance Suppression Based on Adaptive Predictive Control in Weak Grid Condition," *IEEE Journal of Emerging and Selected Topics in Industrial Electronics,* vol. 3, no. 3, pp. 809-820, 2022.

[26] W. Dan, T. Fen, J. C. Vasquez, and J. M. Guerrero, "Control and analysis of droop and reverse droop controllers for distributed generations," in *2014 IEEE 11th International Multi-Conference on Systems, Signals & Devices (SSD14)*, 11-14 Feb. 2014 2014, pp. 1-5.

[27] J. Liu, Y. Miura, and T. Ise, "Comparison of dynamic characteristics between virtual synchronous generator and droop control in inverter-based distributed generators," *IEEE Transactions on Power Electronics,* vol. 31, no. 5, pp. 3600-3611, 2015.

[28] S. D'Arco and J. A. Suul, "Virtual synchronous machines—Classification of implementations and analysis of equivalence to droop controllers for microgrids," in *2013 IEEE Grenoble Conference*, 2013: IEEE, pp. 1-7.

Silvanus D'silva (S'18) He received his Bachelors in Electronics and Telecommunication Engineering from University of Mumbai, India (MU). He obtained his M.Sc. in Electrical Engineering from Kansas State University in 2020. Currently, he is pursuing his Ph.D. degree in Electrical Engineering from University of Illinois Chicago.

Mohammad B. Shadmand (M'15-SM'20) received the Ph.D. degree in electrical engineering from Texas A&M University, College Station, TX, USA, in 2015. From 2017 to 2020, he was an Assistant Professor with the Department of Electrical and Computer Engineering, Kansas State University, Manhattan, KS, USA. Since 2020, he is an Assistant Professor with the University of Illinois at Chicago, IL, USA. Dr. Shadmand was awarded Michelle Munson Serban Simu Keystone Research Scholar, Kansas State University in 2017. He was awarded the 2019 IEEE Myron Zucker Faculty-Student Research Grant. He has awarded multiple best paper awards at different IEEE conferences. He is the General Co-Chair of 50th Annual Conference of the IEEE Industrial Electronics Society (IECON 2024), Chicago, IL. He serves as Associate Editor of IEEE Transactions on Industrial Electronics, IEEE Transactions on Industry Application, and IET Renewable Power Generation.

Mohsen Hosseinzadehtaher (S'18) received his M.Sc. degree in electrical engineering from Amirkabir University of Technology, Tehran, Iran, in 2014. He is currently pursuing the Ph.D. degree in Electrical and Computer Engineering Department at University of Illinois at Chicago, USA.

Alireza Zare has received his B.Sc degree in electrical engineering with a focus on power engineering from Shiraz University, Shiraz, Iran, in 2017 . He has received his MS degree at Washington State University, Vancouver, WA, USA in 2020. He has joined the electrical and computer engineering department at the University of Illinois Chicago as a PhD student starting fall 2021.

Ahmad Khan (S'17) received his B.Sc. and M.Sc. degrees in electrical engineering from Qatar University, Doha, Qatar in 2014 and 2017, respectively. He is currently pursuing the Ph.D. degree in Electrical and Computer Engineering Department at University of Illinois at Chicago, IL, Chicago, USA.

Muhammad F. Umar (S'18) received the B.Sc. degree in Electrical engineering from Lahore University of Management Sciences, Pakistan, in 2014. He has done Masters in Electrical Power Engineering from U.S. Pakistan Center for Advanced Studies in Energy, National University of Sciences and Technology, Pakistan in 2018. Currently, he is pursuing the Ph.D. degree at University of Illinois at Chicago, USA.